Materials Today Communications xxx (xxxx) 115467

Contents lists available at ScienceDirect

Materials Today Communications

journal homepage: www.elsevier.com/locate/mtcomm

Engineered multifunctional AgNPs/PVA nanocomposite flexible films: A green-synthesized platform for simultaneous photocatalytic water purification and antimicrobial wound management

Rajitha Kathi [a], G.L. Merlinsheeba [e], Ravi Kali [b], Balaji Padya [b, d], Nitin P. Wasekar [c], Krishnakumar Balu [f], Vijay Morampudi [e], Pawan Kumar Jain [b], Parvathalu Kalakonda [a, g, *]

[a] Smart Nano Material Research Laboratory (SNRL), Department of Physics, Government City College (A), Hyderabad, Telangana 500002, India
[b] Centre for Carbon Materials, International Advanced Research Centre for Powder Metallurgy and New Materials (ARCI), Hyderabad 500005, India
[c] Center for Engineered Coatings, International Advanced Research Centre for Powder Metallurgy and New Materials (ARCI), Hyderabad 500005, India
[d] School of Engineering Sciences and Technology (SEST), University of Hyderabad, Hyderabad 500046, India
[e] Department of Biochemistry, University of Hyderabad, Hyderabad 500046, India
[f] Department of Chemistry, Karpagam Academy of Higher Education (Deemed to be University, Coimbatore, Tamil Nadu 641 021, India
[g] Saveetha School of Engineering, Saveetha Institute of Medical and Technical Sciences (SIMATS), Chennai, Taminadu 602105, India

ARTICLE INFO

Keywords:
Green synthesis
AgNPs/PVA nanocomposite films
Antibacterial activity
Photocatalytic dye degradation
And flexibility

ABSTRACT

The development of flexible, reusable, and eco-friendly materials that address both water pollution and microbial contamination remains a challenge. Here, we report a green-synthesized, flexible silver nanoparticle-polyvinyl alcohol (AgNPs/PVA) nanocomposite foldable film engineered through *Argyreia nervosa* (AN) leaf extracts, achieving dual photocatalytic and antimicrobial functionality through interfacial design. By controlling AgNPs concentration, we demonstrate morphological control from nanowires to spherical nanoparticles (21.4 ± 4.1 nm), directly influencing the optoelectronic properties (SPR at 446 nm tunable optical band gaps). The optimized film (2.4 mg/mL AgNPs) shows 98% photocatalytic degradation of methylene blue (MB) under visible light while exhibiting first-order degradation kinetics. Pristine PVA films used as negative controls showed less than 5% degradation under identical conditions. The AgNPs/PVA nanocomposite flexible film achieves exceptional antibacterial activity against *Escherichia coli (E. coli)*. A formulation containing 2.2 mg/mL of AgNPs exhibits a fourfold enhancement in efficacy over pristine PVA (negative control), comparable to standard gentamicin disks (positive control, 2.4 cm inhibition zone vs. 2.0 cm for our film). Enhanced thermal-mechanical stability and reusability (over 90% activity after 3 cycles) confirm robust polymer nanoparticle integration (nanoconfinement). This dual-function platform enables portable water purification for remote field operations and antimicrobial wound management, bridging sustainable materials design with practical environmental and biomedical needs.

1. Introduction

The escalating global crisis of waterborne pathogens and organic pollutants demands urgent development of multifunctional, sustainable materials capable of simultaneous disinfection and degradation. Conventional inorganic photocatalysts suffer from rigidity and poor processability, limiting their adaptability in real-world applications [1]. Conversely, polymer-based flexible antimicrobial agents, while foldable or flexible, often exhibit negligible photocatalytic activity, restricting their utility in environmental remediation [2,3]. A critical bottleneck lies in conventional synthesis of metal nanoparticles which rely on toxic reductants, generating hazardous by-products, and constraining their biocompatibility [4–8]. AgNPs were selected as the functional filler because of their unique dual capability: (i) surface plasmon resonance enabling visible-light-driven photocatalysis, and (ii) sustained or control release of Ag + ions for broad-spectrum antimicrobial action. Unlike TiO_2 (only photocatalytic) or chitosan (only antibacterial), AgNPs offer synergistic functionality in a single material [9,10]. To bridge this research gap, eco-friendly nanocomposites with dual functionality are ur-

* Corresponding author at: Smart Nano Material Research Laboratory (SNRL), Department of Physics, Government City College (A), Hyderabad, Telangana 500002, India.
E-mail addresses: parvathalu@wpi.edu, Parvathalu.k@gmail.com (P. Kalakonda).

https://doi.org/10.1016/j.mtcomm.2026.115467
Received 9 April 2026; Received in revised form 15 May 2026; Accepted 29 May 2026
2352-4928/

gently needed, prioritizing green synthesis and scalable fabrication [11].

Among numerous flexible polymers, polyvinyl alcohol (PVA) stands out as an ideal host matrix due to its exceptional film-forming ability, tunable mechanical properties, crosslinking, inherent biocompatibility, and hydroxyl-rich structure that facilitates nanoparticle stabilization [13]. Recent studies have demonstrated PVA's ability to stabilize functional AgNPs while retaining mechanical flexibility under cyclic stress [14,15]. However, pristine PVA lacks intrinsic antimicrobial and photocatalytic activity, a critical limitation addressed in this work through the strategic integration of plasmonic NPs, which imparts dual functionality without sacrificing PVA's processability or flexibility [16,17]. Critically, PVA's water solubility enables entirely aqueous, green processing of nanocomposite films, eliminating organic solvents and aligning with sustainable fabrication [18].

Noble metal nanoparticles, particularly silver (Ag), gold (Au), and platinum (Pt), exhibit rich catalytic and antibacterial efficacy due to their strong surface plasmon resonance (SPR) in the visible range, potential antimicrobial, and proven catalytic activity [4,16,19–22]. For PVA nanocomposites, controlling AgNPs dispersion and distribution, and interfacial interactions are crucial to enhance SPR photocatalysis and sustained release of metal ions [23–25]. Recent work on Ag-Au and Ag-Cu show superior antibacterial and photocatalytic performance due to synergistic effects and enhanced reactive oxygen species (ROS) generation [26–29]. The incorporation of such nanoparticles into PVA matrices has been shown to improve mechanical strength without compromising flexibility, owing to effective stress transfer at the polymer-nanoparticle interface [25,30,31]. Furthermore, the nanoconfinement effect in polymer nanocomposites facilitates sustained ion release, prolonging controllable antibacterial activity while minimizing cytotoxicity [25,32,33]. Recent advances highlight that well-dispersed AgNPs in PVA matrix enhance ROS generation under light irradiation, synergistically boosting photocatalytic degradation of organic pollutants [34–36]. However, achieving morphological control and dual functionality through green synthesis remains challenge [37]. Thus, optimizing AgNPs size and distribution within PVA polymer matrix presents a promising strategy for developing multifunctional composite materials with applications in biomedical devices, environmental remediation, and flexible electronics [38].

To fill this gap, we developed a flexible AgNPs/PVA film using a fully green route [4,9,25,39]. While previous studies have reported AgNPs/PVA composites, most suffer from two major limitations: (1) reliance on toxic chemical reductants, and (2) loss of flexibility or reusability due to uncontrolled nanoparticle aggregation. Furthermore, existing works focus either on water purification or antibacterial activity, rarely both. Our work bridges this gap by using green synthesis to control interfacial interactions, achieving a flexible, reusable, and truly dual-function platform. The AN leaf extract acts as reducing agent, capping agent for morphology control (nanowires to nanospheres), and interfacial binder to PVA. We varied AgNPs from 1 to 2.4 mg/mL and studied the effects on morphology, optical properties, thermal and mechanical behavior, antibacterial activity against E. coli, and photocatalytic degradation of MB dye. The optimized film kills E. coli as effectively as gentamicin and degrades 98% of MB dye in 90 min under visible light. The composite film remains flexible, reusable, and suitable for water purification or wound dressing applications.

2. Materials and characterizations

2.1. Materials and synthesis process

All chemicals and solvents were purchased from Sigma Aldrich Bangalore, India. Silver nitrate ($AgNO_3$, ≥99.5%, Product No. 209139) and polyvinyl alcohol (PVA) granules (Mw ~89,000–98,000, 99% hydrolysed, Product No. 363138) were used as received. Argyreia nervosa (AN) were collected from a medicinal garden in Hyderabad, India. Fresh leaves were rinsed with distilled water, air-dried, and then pulverized into a fine powder (2 g). The fine powder was then added 50 mL of boiled DI water at 75 ^{0}C to prepare the AN green extract solution. The extract was filtered using Whatman filter paper (125 mm) to obtain a clear solution, which was used as the reducing agent for synthesizing & stabilizing silver nanoparticles (AgNPs).

For the synthesis, 0.05 M $AgNO_3$ solution was prepared in 100 mL DI water, and the solution was stirred at 550 rpm and then heated to 90 ^{0}C for 30 min [9]. The clear filtrate of the *AN* extract was introduced dropwise into the vigorously stirred $AgNO_3$ solution. The immediate appearance of a characteristic yellowish-brown confirmed the reduction of silver ions and the successful fabrication of AgNPs. This colloidal suspension was subsequently incubated at room temperature for direct use in subsequent steps without further purification.

A 1% (w/v) aqueous PVA matrix was formulated by dissolving 2 g of PVA granules (Sigma-Aldrich, Bangalore) in 100 mL of deionized water. Complete polymer dissolution was achieved through continuous agitation at 550 rpm while maintaining the solution at 90°C for 30 min. Varying quantities of the freshly synthesized AgNPs colloidal dispersion were then incorporated into the PVA solution. Three AgNP concentrations (1, 2, and 2.4 mg/mL) were selected based on preliminary optimization: below 1 mg/mL, photocatalytic activity was negligible (< 40% degradation); above 2.4 mg/mL, AgNP aggregation caused film brittleness and loss of flexibility. The intermediate 2 mg/mL represents the percolation threshold for optimal interfacial contact without saturation. The composite mixtures were subjected to vigorous agitation at 90–100 °C for 20 min to facilitate a homogeneous and thermal crosslinking of AgNPs throughout the polymer matrix. The colloidal AgNPs concentrations with 1, 2, 2.2, and 2.4 mg/mL were used to make fabricate AgNPs/PVA composite (1 wt% PVA and AgNPs solutions ratio with 1:1). The resulting composite solution was deposited onto glass substrates using a solution-casting technique and allowed to solidify under ambient conditions. Upon complete solvent evaporation, the free-standing nanocomposite films were delaminated from the substrates for subsequent analysis. All synthesis and film fabrication steps were performed in triplicate. Fig. 1 schematically summarizes the overall fabrication protocol for the AgNPs/PVA films and drop-casted films were sown in Fig.S1.

PVA was selected as the polymer matrix due to its unique combination of aqueous processability, film-forming ability, biocompatibility, and capacity to stabilize nanoparticles, making it ideal for green fabrication of reusable functional films. The films were thermally crosslinked during fabrication, which, together with strong AgNPs/PVA interactions, imparted sufficient water stability to allow immersion in aqueous media without dissolution throughout photocatalytic testing.

2.2. Characterization

2.2.1. UV–visible spectroscopy

UV-Vis spectroscopy was used to identify and confirm the formation of AgNPs, identify the surface plasmon resonance (SPR) [40] band, and estimate the direct and indirect optical energy gap of the AgNPs/PVA nanocomposite films. Spectral data were acquired between 200 and 800 nm, referenced against a deionized water blank.

2.2.2. FTIR (Fourier transform infrared spectroscopy)

The surface chemistry of the biosynthesized AgNPs was characterized by FTIR spectroscopy. The raw data analysis was conducted on a Thermo Scientific iS5 spectrometer, collecting spectra from 400 to 4000 cm^{-1} to identify the functional groups from the *AN* extract involved in nanoparticle reduction and capping.

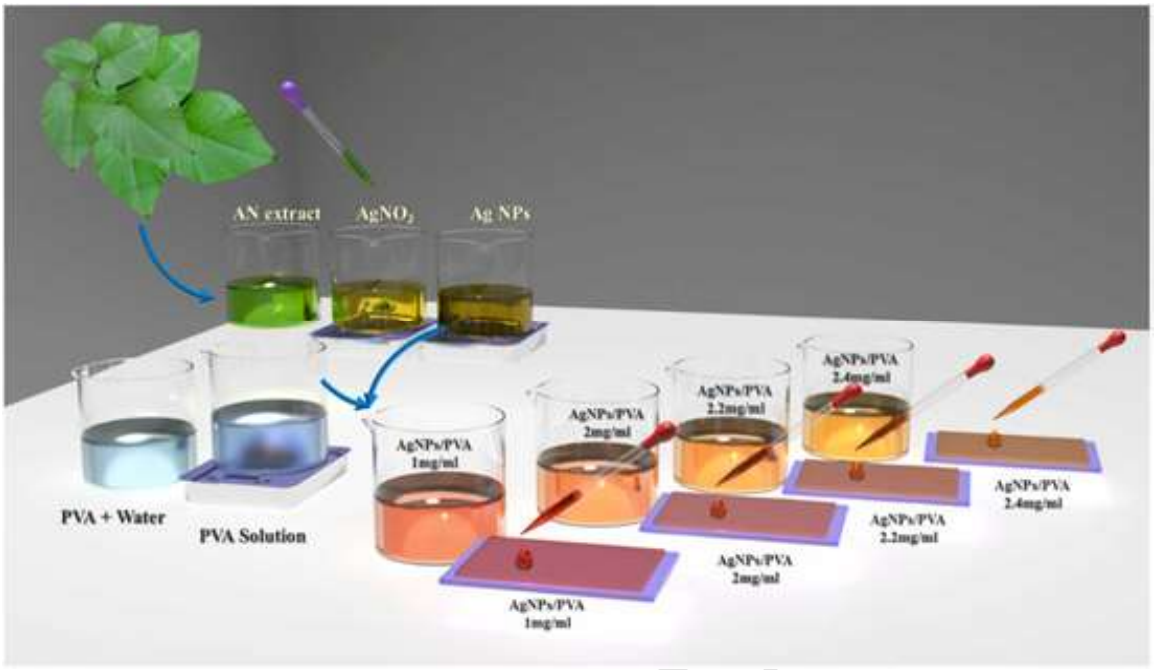

Fig. 1. Illustration of the bio- synthesis and fabrication process for AgNPs/PVA nanocomposite films. The process involves (i) the reduction of silver ions (Ag^{+}) to AgNPs using *AN* leaf extract, and (ii) the integration of the resulting AgNPs colloidal solution at varying concentrations into a polyvinyl alcohol (PVA) matrix, followed by solution casting to form flexible, free-standing films.

2.2.3. XRD (X-Ray diffraction) analysis

XRD with Cu-Kα radiation was utilized to estimate the crystalline nature and crystallite dimensions of the AgNPs/PVA composite films [41]. Scans were performed across a 2θ range of 20–80°. The average crystallite size of the AgNPs was derived by applying the Debye-Scherrer equation for the most intense diffraction peak, using a Scherrer constant of 0.9 and the wavelength of the Cu-Kα source.

2.2.4. SEM (Scanning electron microscopy)

A ZEISS field FE-SEM was used to examine the surface topology details and NPs distribution within the AgNPs/PVA nanocomposite films across a range of AgNPs loadings. Particle size distribution analysis was performed using ImageJ software (NIH) on FE-SEM micrographs. For each sample, over 100 individual nanoparticles/nanostructures were measured from multiple images to ensure statistical significance. While this study does not include direct surface analysis via EDX, the uniform distribution and strong adhesion of AgNPs within the PVA matrix were indirectly confirmed through macroscopic, optical, and functional consistency across the films. The sustained photocatalytic and antibacterial performance, along with the film's structural integrity over multiple reuse cycles, collectively support the homogeneous integration and stability of AgNPs in the composite.

2.2.5. DSC (Differential scanning calorimetry)

The thermal behaviour of neat PVA and its silver nanocomposites was investigated using differential scanning calorimetry (TA Instruments Q20 DSC) [40]. Samples weighing approximately 2 mg were encapsulated in hermetically sealed aluminum crucibles, using an empty crucible as reference. The analysis was conducted under nitrogen atmosphere (50 mL/min flow rate) with a temperature ramp from 30 to 250 °C at a heating rate of 10 °C/min. The melting temperature (T_m) was determined at the endothermic peak minimum. Crystallinity percentage was quantified using the relationship $X = (\Delta H_m / 138.6\ J/g) \times 100\%$, where ΔH_m represents the experimental melting enthalpy and 138.6 J/g denotes the theoretical value for fully crystalline PVA. Triplicate runs confirmed measurement reproducibility.

2.2.6. TGA (Thermogravimetric analysis)

The thermal degradation behaviour of pure PVA and AgNPs/PVA nanocomposites was analyzed using a thermogravimetric analyzer (TGA Q50, TA Instruments). Samples (2.0 ± 0.05 mg) were loaded into open platinum crucibles. Thermal degradation profiles were recorded under a nitrogen purge (40 mL min^{-1}) with a temperature ramp from 30 to 800 °C at 10 °C min^{-1} . Key thermal stability parameters, including the onset decomposition temperature and the maximum degradation rate, were derived from the corresponding derivative thermogravimetric (DTG) curves. The residual mass at 800 °C was recorded to assess thermal stability. All measurements were performed in triplicate, and blank corrections were applied using data from an empty crucible run under identical conditions. Temperature calibration was verified using a high-purity nickel standard (Curie point = 354 °C), and mass calibration was performed using certified reference materials. Results are presented as mean ± standard deviation from three independent measurements.

The composite mixtures were heated at different temperatures in open air and heat treatment causes partial dehydration of adjacent PVA chains, leading to the formation of intermolecular ether bonds ($–CH_2–O–CH_2–$) through condensation of hydroxyl groups. This thermally induced crosslinking creates a three-dimensional network that renders the film insoluble in water. The thermal crosslinking was performed at 95 ± 2°C for 20 min in open air [42]. Under these conditions, partial dehydration of adjacent PVA hydroxyl groups leads to intermolecular ether bond formation ($-CH_2-O-CH_2-$) via condensation, creating a three-dimensional network that renders the film insoluble in water [43]. This temperature is well below the degradation onset of PVA (~220°C) but sufficiently high to promote chain mobility and hydroxyl group condensation [44].

2.2.7. Micro-tensile testing

We determined the tensile properties of the nanocomposite films using an Instron 5944 micro-tensile tester in accordance with ASTM D638 Type-V standards [45]. Dog-bone-shaped specimens were cut using a computer-controlled laser cutter with a standardized gauge length of 10.0 ± 0.1 mm. Prior to testing, all samples were conditioned for 24 h at 25.0 ± 0.5 °C and 50 ± 2% relative humidity. Mechanical evaluation employed a constant crosshead speed of 5.0 mm/min with a 0.10 N pre-load to eliminate specimen slack. The elastic modulus was calculated from the stress-strain curve's linear segment (0.1–0.5% strain range), while ultimate tensile strength and elongation at break were recorded at fracture initiation. Results represent the average of three separate measurements for each composition, expressed as mean ± standard deviation.

2.3. Antibacterial activity

The antibacterial efficacy was evaluated for the freestanding PVA, AgNPs/PVA nanocomposite films to assess their performance as solid-state functional materials.

2.3.1. Disk diffusion

Antibacterial activity of the AgNPs/PVA nanocomposite films was assessed against enteropathogenic *E. coli* (EPEC, O127:H6) via disk diffusion method. A bacterial suspension standardized to 0.5 McFarland was uniformly seeded onto Mueller-Hinton agar [46]. Sterilized 6-mm discs of the composite films were then applied to the inoculated surface. Control experiments included 30 μg gentamicin discs (positive control) and sterile LB medium (negative control). Following 24-hour aerobic incubation at 37 °C, the diameters of the inhibition zones, inclusive of the disc, were measured with 0.1 mm precision. The experiment was conducted in triplicate. The disk diffusion method was selected for its reliability in screening antimicrobial activity of solid materials and compatibility with film-based samples.

2.3.2. Minimum inhibition concentration (MIC) assay

A quantitative broth microdilution technique was adapted to determine the antimicrobial potency of the AgNPs/PVA nanocomposite films [42]. Sterile 5 × 5 mm film squares were introduced into wells of a 96-well plate prefilled with 200 μL of LB broth containing a standardized inoculum of EPEC. A two-fold serial dilution series was generated by transferring film specimens sequentially to subsequent wells containing freshly inoculated medium. Following 6 h of static incubation at 37 °C, bacterial growth inhibition was evaluated both by visual inspection and optical density measurements at 600 nm. The MIC was designated as the lowest film loading that prevented visibility growth, with confirmation achieved by subculturing the well contents on LB agar and assessing colony forming units (CFU). Pristine PVA films and a 2 μg/mL gentamicin solution functioned as negative and positive controls, respectively [47]. The entire procedure was executed with three biological replicates, each comprising technical triplicates.

2.4. Photocatalytic activity

The degradation of MB dye under visible light served as a standard protocol reaction to probe the photocatalytic performance of the AgNPs/PVA nanocomposites. In a typical experiment, a film with 2.4 mg/mL AgNPs loading was immersed in 10 mg L^{-1} aqueous MB solution. An initial 15-minute dark period ensured the establishment of adsorption-desorption equilibrium prior to illumination with a 10 W LED source ($\lambda \geq 400$ nm) with constant agitation. Samples were taken every 30 min during irradiation, centrifuged to remove particulates, and their absorbance at 664 nm was measured via UV-Vis spectroscopy. Photocatalytic efficiency was determined using the relationship: Degradation (%) = $[(A_0 - A_t)/A_0] \times 100$, where A_0 and A_t signify the initial and time-dependent absorbance, respectively. The essential photocatalytic function of the AgNPs was verified by control tests with pristine PVA films. Although PVA is water-soluble, the films exhibited excellent aqueous stability during testing due to thermal crosslinking during fabrication and strong interactions between AgNPs and the polymer matrix. This prevented dissolution and enabled repeated use without structural failure. The stability of composite film is crucial for reusable photocatalytic applications and distinguishes our film design from conventional soluble PVA formats.

2.5. Green synthesis metrics and quality assurance & quality control

We calculated a synthesis metrics to claim of green synthesis (Table.S1). The atom economy came out to about 86.5%, meaning most of what we put into the reaction ended up as useful product. The E-factor, which measures waste relative to product, was 3.2. For comparison, anything below 5 is considered acceptable for green processes, and conventional nanoparticle synthesis often gives values above 10. We used only water as the solvent, no DMF, no THF, no organic solvents at all. And instead of toxic chemicals like $NaBH_4$ or hydrazine, we used *Argyreia nervosa* leaf extract to reduce and stabilize the silver nanoparticles [10]. That means no hazardous chemical waste from reducing agents or stabilizers.

For UV-Vis, we ran a blank with deionized water and scanned each sample triplicate. For FTIR, we did a background correction before each run and collected 32 scans per sample at 4 cm^{-1} resolution. For XRD, we calibrated the instrument with a silicon standard ($2\theta = 28.44°$). For SEM, we measured more than 100 particles from different areas of each sample. For DSC, we calibrated the temperature using an indium standard (156.6°C). For TGA, we used a nickel standard (354°C) for calibration and applied blank correction. For tensile testing, we calibrated the load cell with certified weights and conditioned the samples at 25°C and 50% relative humidity for 24 h before testing. In this synthesis process, the main challenges are batch-to-batch variation in leaf extract and making large uniform films. Dried standardized leaf powder can fix the first problem. Roll-to-roll coating can fix the second. With these changes, practical use is possible and more economical.

3. Results and discussion

UV-Vis absorption spectra of the AgNPs/PVA nanocomposite films showed a strong dependence on AgNPs concentration. The film with a lower AgNPs concentration (1 mg/mL) exhibited a single, broad absorption peak centered at ~282 nm, which corresponds to the intrinsic absorption of the PVA matrix. In contrast, the nanocomposite with a higher AgNPs loading (2.4 mg/mL) showed a significantly intensified and broadened absorption, along with a distinct surface plasmon resonance (SPR) band centred at 446 nm [48,49] (Fig.2) and this characteristic SPR band confirms the presence of well-defined AgNPs and indicates the collective oscillation of surface electrons. This SPR feature arises from collective electron oscillations on the surface of AgNPs, reflecting their increased population and interparticle coupling at higher AgNPs concentration. The increased intensity and broadening of the SPR band at higher concentration suggest a greater population of AgNPs with enhanced interparticle coupling, which may indicate some aggregation or a broader size distribution.

Tauc plot analysis (Fig. 3) revealed a concentration-dependent narrowing of the optical band gap [50] in the AgNPs/PVA nanocomposites. The direct and indirect band gaps estimated 3.3 eV and 2.7 eV respectively for the film containing 1 mg/mL AgNPs. A systematic narrowing was observed at the higher loading of 2.4 mg/mL, where the band gaps decreased to 2.7 eV (direct) and 2.3 eV (indirect). The narrowing of the band gap can be attributed to enhanced electronic interactions at the AgNPs-PVA interface, which facilitate charge carrier delocalization and introduce new electronic states within the band structure of the

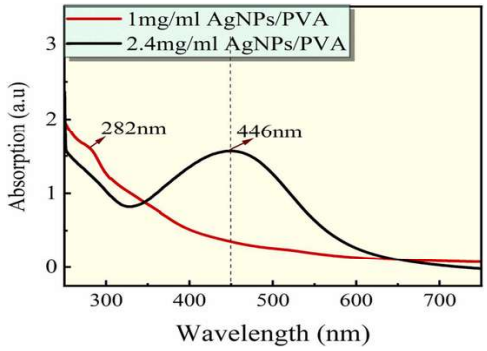

Fig. 2. UV-Vis absorption spectra of AgNPs/PVA nanocomposite films, comparing the distinct optical properties at AgNPs concentrations of 1.0 mg/mL and 2.4 mg/mL. The intensified and broadened SPR band at the higher loading indicates a greater nanoparticle density and potential interparticle coupling.

nanocomposite. This trend aligns with quantum confinement effects and the introduction of impurity states associated with the AgNPs. The systematic tunability of the band gap with AgNPs concentration demonstrates the potential to engineer the optoelectronic properties of the nanocomposite for applications in photonics, sensing, and advanced optoelectronics.

FTIR analysis of the AN leaf extract mediated AgNPs confirmed the involvement of specific phytochemical functional groups in the reduction of Ag^+ ions and stabilization of the resulting NPs (Fig. 4**).** The spectrum of the AN aqueous extract showed similar characteristic transmission bands at 3308, 1628, and 594 cm^{-1} . The broad band at 3308 cm^{-1} in the AN extract is characteristic of O–H stretching vibrations from polyphenols and flavonoids [51], while the sharp band at 1628 cm^{-1} corresponds to C═O stretching (amide I) and/or C═C stretching in aromatic rings. The suppression and shifting of these specific bands in the AN-AgNPs spectrum confirm that hydroxyl groups (–OH) and carbonyl groups (C═O) are instrumental in reducing Ag^+ ions and capping the newly formed nanoparticles. The abundance of phenolic compounds in the AN extract provides powerful antioxidant activity, facilitating the reduction of metal ions. Thus, the biomolecules in the AN extract serve a dual function: as reducing agents for Ag^+ ions and as capping agents to stabilize the AgNPs, preventing aggregation.

Fig. 5 presents FE-SEM micrographs illustrating the morphological evolution of AgNPs within the PVA matrix at different loadings accompanied, by quantitative size distribution histograms obtained from Image J analysis of over 100 particles per condition. At the lower concentration (1 mg/mL, Fig. 5**A, B**), the nanocomposite exhibited predominantly anisotropic structure, resulting nanowire structures with **diameter 28.6 ± 3.2 nm and length of several micrometres (15–25 μm).** This morphology suggests a less restricted growth environment where the lower density of nucleation sites allows for preferential growth along certain crystallographic directions.

At an optimum concentration (2.2 mg/mL, Fig. 5**C, D**), the nanostructures shape shifted to predominantly **spherical nanoparticles with an average diameter of 21.4 ± 4.1 nm**, with a notable increase in particle density and a reduction in average size, likely due to spatial constraints within the polymer matrix that suppressed anisotropic growth. At the highest loading (2.4 mg/mL, Fig. 5**E, F**), while individual spherical nanoparticles with diameters in the 20–30 nm range are still discernible at higher magnifications, there is pronounced aggregation and coalescence into larger clusters. The size distribution analysis reveals a distribution with peaks corresponding to primary nanoparticles (~25 nm) and larger aggregates (50–100 nm). This aggregation is likely due to reduced inter-particle distance at high nanoparticle density, leading to increased van der Waals interactions and possible bridging by PVA chains. The analysis of diameter at different loadings of AgNPs within the polymer matrix is shown in the Fig.S2 (supplementary Figure). In summary, the morphology transitioned from well-dispersed nanowires at lower concentrations to densely packed spherical nanoparticles and ultimately to a coalesced, aggregated structure as the AgNPs loading increased.

XRD patterns confirmed the presence of crystalline silver nanoparticles uniformly distributed throughout the PVA matrix in all composite formulations (Fig. 6). Distinct diffraction peaks observed at 2θ values of 38.2°, 46.0°, 64.5°, and 77.5° align with the (111), (200), (220), and (311) planes of FCC silver, respectively (JCPDS 04–0783) [46]. The average crystallite size, calculated using the Debye–Scherrer equation applied to the (111) peak for the **2.4 mg/mL AgNPs/PVA film**, was found to be **26.3 nm**, as confirmed by FE-SEM [24,52]. This confirm and aligns with FE-SEM observations. Furthermore, the progressive enhancement in peak intensity, particularly for the (111) plane, with increasing AgNPs concentration signifies improved crystallinity at higher nanoparticle loadings.

The thermal behavior of pristine PVA and AgNPs/PVA nanocomposites was analyzed using DSC, as shown in Fig. 7**.** The pristine PVA film showed a sharp endothermic peak at approximately 225 °C, corresponding to its melting temperature (T_m). Upon incorporation of AgNPs, the melting peak broadened and shifted to lower temperatures (~220 °C), with the magnitude of this shift and a decrease in peak intensity becoming more pronounced at higher AgNPs loadings (from 1 to 2.4 mg/mL). These observations suggest that the AgNPs act as a disruptor of the PVA crystalline domains, reducing overall crystallinity and hindering polymer chain mobility during melting. The consistent trend of altered thermal transitions across the tested AgNPs loadings **(0, 1, 2**

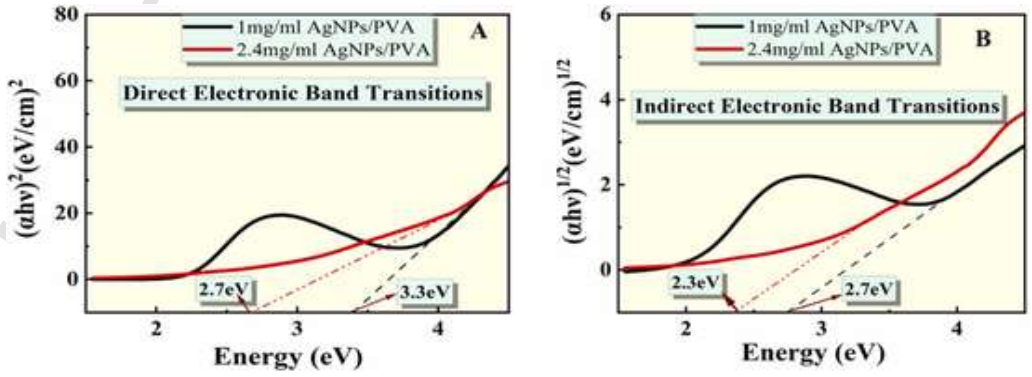

Fig.3. Tauc plots were used to calculate how much energy is needed to activate the silver nanoparticle films. They show how adding more silver nanoparticles changes this required energy.

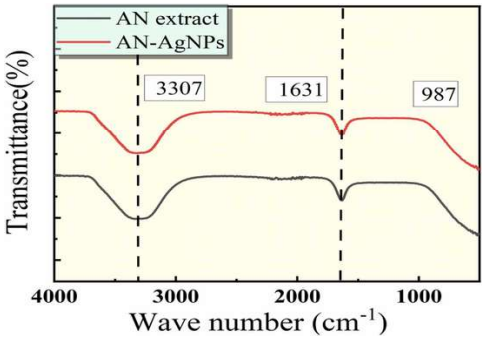

Fig.4. FTIR spectra of AN leaf extract and AN-mediated AgNPs, identifying the similar functional groups of biomolecules.

& 2.2: showed similar trend, and 2.4 mg/mL) confirms their successful incorporation and dispersion within the PVA matrix, effectively tailoring the thermal properties of the nanocomposite.

The thermal stability and decomposition behaviour of pristine PVA and 2.4 mg/mL AgNPs/PVA nanocomposites were investigated by TGA, as presented in Fig. 8**.** Presenting only the two most representative datasets (pristine PVA and the highest-performing composite) avoids visual clutter and allows the reader to focus on the most important contrast the **onset of degradation and the final char yield**. The full thermogravimetric analysis for all AgNPs loadings (0, 1.0, 2.0, 2.2, and 2.4 mg/mL) is provided in Supplementary Fig. S3, confirming the concentration-dependent enhancement in thermal stability. Thermogravimetric profile of pristine PVA indicated a two-stage mass loss: an initial minor event below 100 °C from moisture evolution, succeeded by the primary polymer backbone degradation initiating near 270 °C. For the AgNPs/PVA composites, the onset temperature of the major decomposition step shifted to progressively higher temperatures with increasing AgNPs loading, indicating enhanced thermal stability. Furthermore, the residual mass at 800 °C increased systematically with AgNPs concentration, confirming the presence of non-volatile silver nanoparticles within the polymer matrix. These results demonstrate that the incorporation of AgNPs enhances the thermal resistance of the PVA matrix by delaying the onset of polymer degradation and increasing the char residue, thereby imparting improved thermal stability to the nanocomposite.

Tensile tests, summarized in Fig. 9 and supplementary Table.S2, revealed the reinforcing effect of AgNPs on the PVA matrix. Pristine PVA demonstrated characteristic flexibility with a ultimate tensile strength (UTS) of 12 ± 2 MPa and modulus of 6 ± 0.5 MPa. The UTS and tensile modulus increases as function of AgNPs (1, 2.2, and 2.4 mg/mL) loadings. This enhancement is attributed to a reinforcing mechanism where the well-dispersed AgNPs, strongly adhered to the matrix via phytochemical capping, restrict polymer chain mobility and facilitate efficient stress transfer. The nanocomposite with the highest AgNPs loading (2.4 mg/mL) demonstrated the most substantial improvement, with an elastic modulus of 45 ± 3 MPa and a UTS of 323 ± 8 MPa (± SD, n = 3), representing the highest mechanical reinforcement. This enhancement might be due to well-dispersed AgNPs within the polymer matrix restrict the polymer chain mobility and facilitate stress transfer through hydrogen bonding between phytochemical capping agents & PVA hydroxyl groups. These findings confirm that increasing the AgNPs concentration effectively strengthens the nanocomposite by enhancing both stiffness and tensile strength.

3.1. Antibacterial activity and mechanism of film based AgNPs/PVA composites

Fig.10a **(A)** presents the antibacterial efficacy of pristine PVA and AgNPs/PVA nanocomposite films against E. coli, as determined by a disk diffusion assay. The AgNPs/PVA composite film with a 2.2 mg/mL AgNPs loading exhibited pronounced antibacterial activity, producing an inhibition zone of **2 cm**, which was comparable to the standard antibiotic gentamicin (**2.4 cm**). However, a further increase in AgNPs loading to 2.4 mg/mL resulted in a smaller inhibition zone of **1.5 cm**. This reduction in efficacy at the highest concentration is likely attributed to increase AgNPs aggregation and denser composite matrix (as seen in Fig.5**E, F**), which can restrict the diffusion and release of Ag^+ ions into surrounding region. This demonstrates that for film-based applications, an optimal nanoparticle loading exists to balance antimicrobial content with release kinetics. In contrast, pristine PVA films and the composite with 1 mg/mL AgNPs loading showed no detectable inhibition zones, indicating that the Ag^+ ion concentration was below the threshold required for significant antibacterial action (shown in Fig. 10a (B**)**). The primary antibacterial mechanism of AgNPs involves the release of Ag^+ ions, which can adhere to and disrupt the bacterial cell wall and membrane, compromising their integrity and impairing vital functions such as ATP production [53]. Furthermore, internalized Ag^+ ions can inactivate essential intracellular components, including enzymes and DNA, and induce oxidative stress through the generation of ROS [54].

Fig. 10b **(A &B)** shows the quantitative antibacterial activity of pristine PVA and AgNPs/PVA composite films, as determined by a minimum inhibitory concentration (MIC) assay. The MIC assay provides a quantitative measure of antibacterial activity. In this assay, a broth culture of *E. coli* was exposed to the films, followed by incubation for 6 h at 37 °C. The MIC was estimated by quantifying bacterial growth via optical density measurements at 600 nm. Pristine PVA films and the composite with 2.2 mg/mL AgNPs showed minimal antibacterial activity. In the disk diffusion assay (Fig. 10b**(A)**), a faint inhibition zone was observed for the 2.2 mg/mL composite, indicating trace release of Ag^+ ions. However, in the quantitative MIC assay (Fig. 10b **(B)**), the same film exhibited a high MIC value, confirming that the Ag^+ concentration was insufficient to fully inhibit bacterial growth in liquid culture. This difference highlights the higher sensitivity of the disk diffusion assay for detecting low-level antimicrobial activity, while the MIC assay provides a more stringent measure of bactericidal potency. These results highlight the potential of flexible film-based nanocomposites for applications requiring antibacterial properties, such as food packaging and wound dressings.

This study demonstrates a controlled antibacterial release mechanism utilizing pristine PVA and AgNPs/PVA composite films in a disk format, a method that offers distinct advantages over conventional solution-based approaches (Supplementary Fig.S4**,** Table S3). While pristine PVA films showed no bactericidal effect, the AgNPs/PVA composites enabled a sustained release of Ag^+ ions upon hydration. We propose that the controlled release of Ag^+ ions penetrate the bacterial cell envelope and bind to vital intracellular components, including sulfur-containing proteins in the electron transport chain (affecting ATP synthesis) and nucleic acids [47]. This binding induces structural denaturation and functional disruption of these biomolecules, leading to the collapse of metabolic pathways and inhibition of genetic replication. The resultant irreversible cellular damage and loss of viability confirm that the sustained ion release from the film matrix, coupled with targeted intracellular action, provides a reliable and effective antibacterial mechanism, effectively demonstrated by this film disk-based methodology.

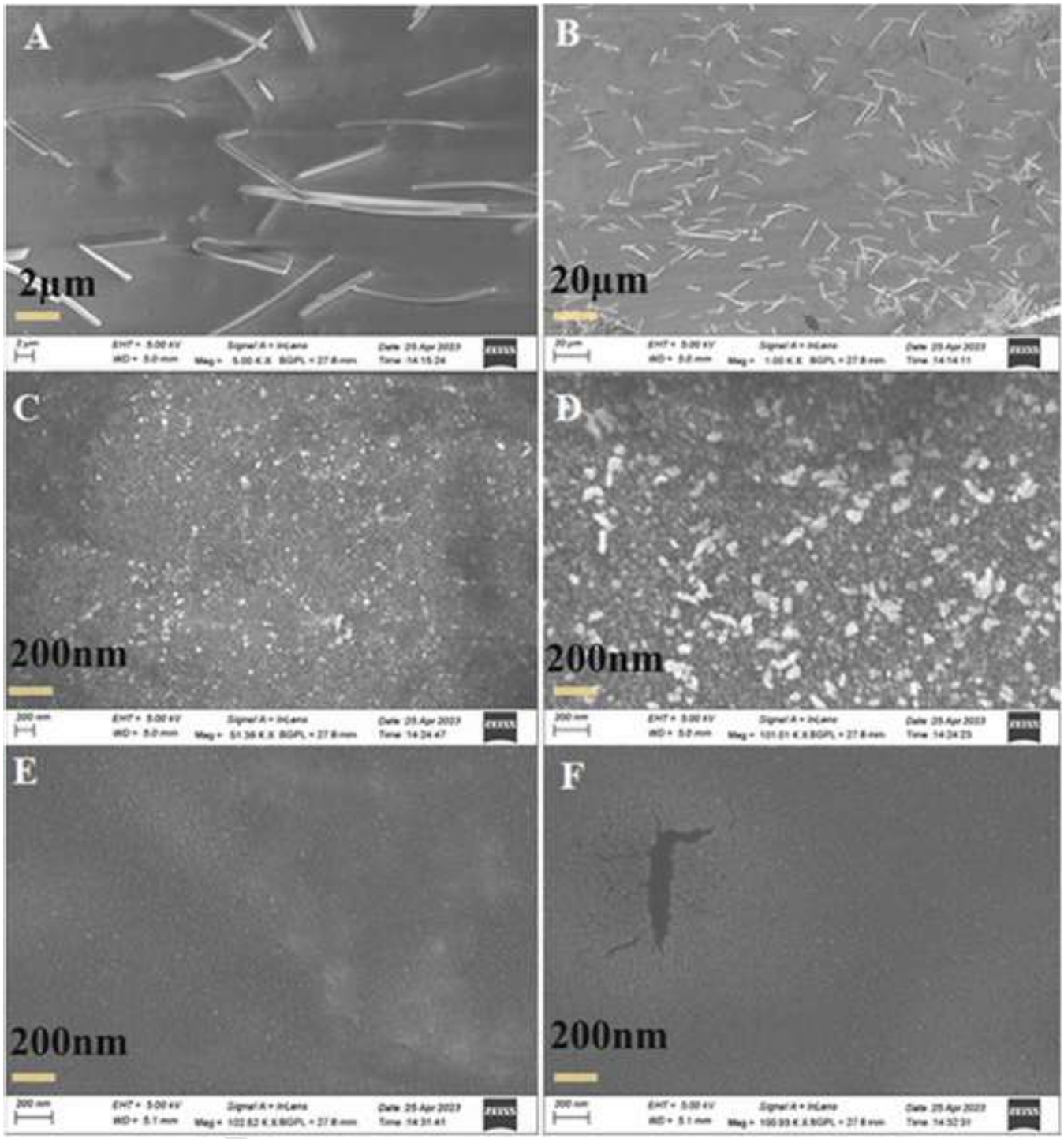

Fig. 5. FE-SEM analysis of AN-mediated AgNPs/PVA films showing surface morphology evolution and quantitative size distribution across AgNPs loadings: (A,B) 1.0 mg/mL showing nanowire morphology with diameter distribution histogram (inset), (C,D) 2.2 mg/mL showing spherical nanoparticles with size distribution histogram (inset), (E,F) 2.4 mg/mL showing aggregated nanoparticles.

3.2. Photocatalysis-dye degradation and mechanism of film based AgNPs/PVA composites

We assessed the photocatalytic efficiency of the AgNPs/PVA nanocomposite films by tracking the decolorization of MB under visible light. The film with 2.4 mg/mL AgNPs loading was identified as the optimal catalyst. Fig. 11 shows the time-dependent UV-Vis spectral changes of an aqueous MB solution (10 mg L^{-1}) in the presence of a 3 × 3 mm AgNPs/PVA (2.4 mg/mL) film. To account for preliminary adsorption, the reaction system was equilibrated in the dark for 15 min prior to illumination. Photocatalysis was then initiated using a 10 W visible light source ($\lambda \geq 400$ nm), with 3 mL samples collected at 20-minute intervals. A steady decline in the 664 nm absorption band provided direct evidence of methylene blue degradation, culminating in near-total decolorization (≥98%) within 90 min. Our film's photocatalytic efficiency (98%) and antibacterial performance (comparable to

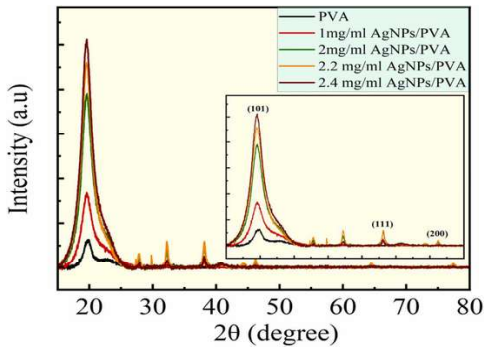

Fig. 6. X-ray diffraction patterns of *Argyreia nervosa*-mediated AgNPs/PVA nanocomposite films, showing the evolution of face-centered cubic silver crystalline phases with increasing AgNPs concentration. The intensified (111) peak at higher loadings confirms enhanced crystallinity.

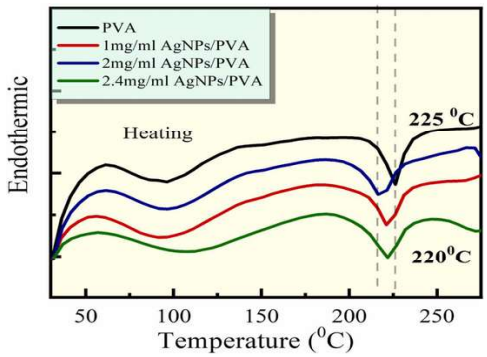

Fig. 7. Differential scanning calorimetry (DSC) thermograms of pristine PVA and *Argyreia nervosa*-mediated AgNPs/PVA nanocomposite films (0, 1, 2, 2.4 mg/mL), showing the effect of AgNPs concentration on the melting transition and crystallinity of the polymer matrix.

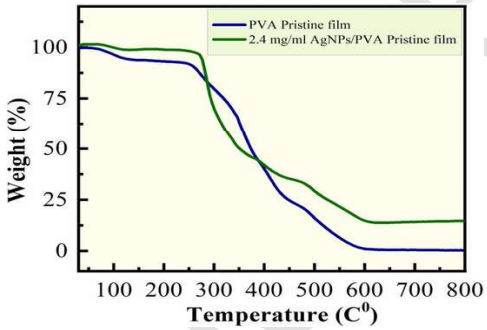

Fig. 8. Thermal degradation profiles of pristine PVA and the AgNPs/PVA nanocomposite film (2.4 mg/mL), demonstrating improved thermal stability through a delayed decomposition onset and a higher char yield.

gentamicin) compare favorably with recent AgNPs/polymer composites [5,39,55,56], while offering the added advantage of green synthesis and morphological tunability. Control experiments using pristine PVA films under identical conditions showed negligible MB degradation (<5%), confirming that photocatalytic activity originates solely from AgNPs. Furthermore, the nanocomposite films remained physically intact and retained over 90% of their initial photocatalytic efficiency across three consecutive reuse cycles, demonstrating their structural stability and potential for repeated application in water treatment. This robust performance of the composite material as a viable, reusable catalyst for the treatment of organic contaminants in wastewater.

The temporal progression of MB degradation is presented in Fig. 12a, showing both the decrease in absorption intensity (A) and the corresponding degradation percentage (B). After 90 min of visible light irradiation, the MB absorption approached zero, corresponding to a 98% degradation efficiency. The film-based catalyst design offers distinct advantages over conventional powdered or colloidal systems, including enhanced stability, facile recovery from treated water, and consistent reusability. This integrated design eliminates the need for energy-intensive post-treatment separation steps, addressing a major limitation of powdered catalysts and presenting a more practical solution for sustainable water purification. The maintained structural integrity and robust photocatalytic performance after multiple cycles underscore the potential of these films for scalable environmental remediation applications.

The degradation kinetics of methylene blue (MB) by the AgNPs/PVA nanocomposite films followed *pseudo*-first-order behavior, as evidenced by the linear correlation of $\ln(C_0/C)$ versus irradiation time in Fig. 12b (B). Kinetic processing of the experimental data produced a rate constant of 0.017 min^{-1} with strong correlation (R^2 = 0.954), supporting the model's validity. Fig. 12b (A) illustrates the systematic reduction in normalized MB concentration (C/C_0) over the reaction period, providing visual confirmation of efficient dye breakdown. These kinetic findings quantitatively validate the high photocatalytic performance measured in degradation tests. The close fit to pseudo-first-order kinetics indicate that MB concentration serves as the primary rate-determining factor under these reaction conditions. The degradation kinetics of MB by the AgNPs/PVA nanocomposite films followed *pseudo*-first-order behavior, as evidenced by the linear correlation of $\ln(C_0/C)$ versus irradiation time in Fig. 12b (B). Kinetic processing of the experimental data produced a rate constant of 0.017 min^{-1} with strong correlation (R^2 = 0.954), supporting the model's validity

The photocatalytic efficiency of the AgNPs/PVA film can be further contextualized by comparing its rate constant (**k = 0.017 min^{-1}**) with those of similar green-synthesized AgNPs-based systems reported in recent literature. For instance, biosynthesized Cu–Ag bimetallic nanoparticles exhibited a rate constant of ~0.012 min^{-1} for dye degradation [28], while AgNPs embedded in various polymer matrices typically achieve rate constants in the range of 0.010–0.025 min^{-1} under visible light [35]. The competitive performance of our flexible, solid-state film underscores not only the efficacy of the *AN*-mediated AgNPs but also the practical advantage of the PVA matrix in facilitating a reusable, easily deployable photocatalytic platform.

The flexible AgNPs/PVA nanocomposite films degraded organic dyes under visible-light illumination through a plasmon-driven photocatalytic mechanism (Supplementary Fig. S4, Table S3). The mechanism in Fig. S4 is drawn from our experimental results and existing literature of plasmonic AgNPs. When the catalyst film exposed to visible light, the localized surface plasmon resonance (SPR) of AgNPs was exciting, leading to the collective oscillation of surface electrons. The relaxation of these excited states generated energetic "hot electrons" and complementary positive vacancies ("hot holes") (electrons and holes with higher energy than the Fermi level). The hot electrons were transferred to dissolved oxygen molecules, reducing them to superoxide radical anions ($O_2^{\bullet-}$), which could further transform into highly reactive hydroxyl radicals ($^{\bullet}OH$) [52]. Meanwhile, the hot holes at the nanoparticle surface oxidized water molecules (H_2O/OH^-) or directly attacked dye molecules. The PVA matrix played a stabilizing role by uniformly dispersing the AgNPs and modulating their surface chemistry, which suppressed uncontrolled Ag^+ ion leaching and ensured sustained and controlled ROS generation. Consequently, methylene blue underwent oxidative degradation through stepwise breakdown of aromatic rings and azo linkages, ultimately leading to mineralization into CO_2 and

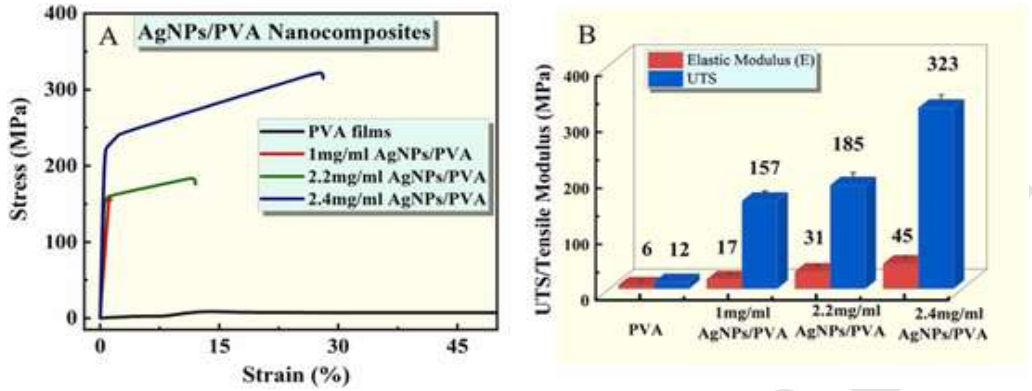

Fig. 9. Tensile properties of AN-mediated AgNPs/PVA nanocomposites. (a) Stress-strain behavior and (b) quantitative comparison of elastic modulus and UTS values across different AgNPs concentrations, showing enhanced mechanical properties at higher loadings.

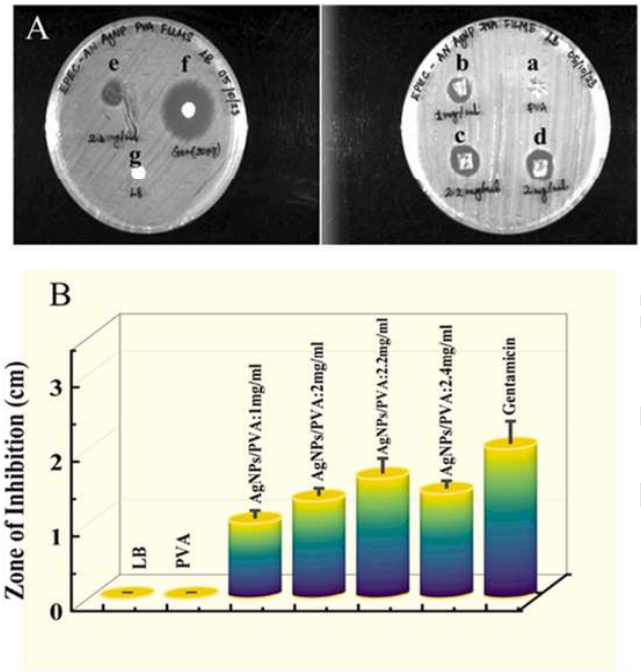

Fig. 10a. Antibacterial activity of *Argyreia nervosa*-mediated AgNPs/PVA nanocomposite films against *E. coli*. (A) Clear image of the agar diffusion assay showing inhibition zones for: (a) pristine PVA, (b) 1 mg/mL AgNPs/PVA film shows a faint inhibition zone, indicating trace antimicrobial activity detectable only in the sensitive disk diffusion assay (c) 2 mg/mL, (d) 2.2 mg/mL, and (e) 2.4 mg/mL AgNPs/PVA films, with (f) gentamicin and (g) LB medium as positive and negative controls, respectively. (B) Quantitative analysis of the inhibition zone diameter, demonstrating a concentration-dependent efficacy that is maximum at 2.2 mg/mL AgNPs loading.

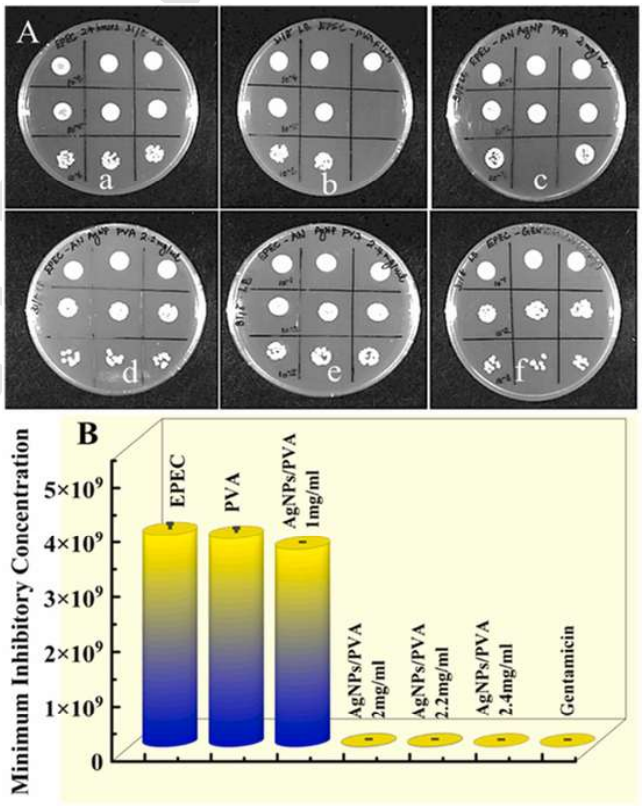

Fig. 10b. Minimum inhibitory concentration (MIC) assessment of *Argyreia nervosa*-mediated AgNPs/PVA nanocomposite films against enteropathogenic *E. coli* (EPEC O127:H6). (A) Colony forming unit (CFU) results showing bacterial growth inhibition for: (a) EPEC control, (b) pristine PVA, (c) 2 mg/mL, (d) 2.2 mg/mL, and (e) 2.4 mg/mL AgNPs/PVA films, with (f) gentamicin as positive control. (B) Quantitative analysis of bacterial viability demonstrating concentration-dependent antibacterial efficacy, with the 2.2 mg/mL AgNPs formulation showing a fourfold enhancement in MIC value compared to control films.

H_2O. The nanostructured interface within the film facilitated efficient charge separation, minimizing electron-hole recombination and thereby enhancing the overall photocatalytic degradation efficiency. This mechanistic pathway enabled complete detoxification of complex organic dyes, rendering the treated water safe for reuse, while the catalyst maintained structural and functional stability over multiple operational cycles. While the proposed mechanism is consistent with our characterization and established literature on plasmonic AgNPs, scavenger experiments to identify specific reactive oxygen species were beyond the scope of this study and are planned for future mechanistic investigation.

4. Conclusion

We successfully fabricated flexible AgNPs/PVA nanocomposite films using a green synthesis route with AN extract, achieving unprece-

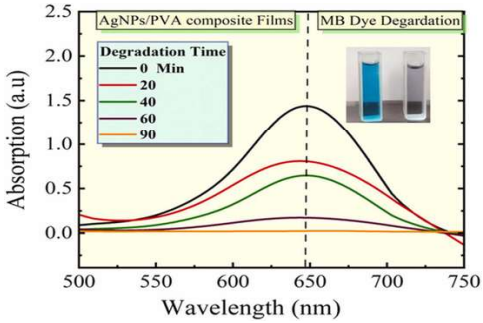

Fig. 11. Photocatalytic degradation of MB dye using *Argyreia nervosa*-mediated AgNPs/PVA nanocomposite films (2.4 mg/mL) under visible light irradiation, demonstrating complete dye decolorization within 90 min and confirming the films' effectiveness as reusable photocatalytic platforms.

dented shape control where low AgNP loading (1 mg/mL) produced nanowires of 28.6 ± 3.2 nm diameter while higher concentrations (2.2–2.4 mg/mL) yielded spherical nanoparticles of 21.4 ± 4.1 nm. The optimized films delivered exceptional dual functionality: the 2.2 mg/mL formulation showed antibacterial activity against *E. coli* with inhibition zones matching gentamicin and a low MIC value, while the 2.4 mg/mL film degraded 98% of MB dye under visible light within 90 min following pseudo-first-order kinetics (rate constant 0.017 min^{-1}), competitive with leading AgNP-based systems. Mechanistically, antibacterial action arises from sustained Ag^+ ion control release from the matrix, whereas photocatalysis stems from plasmon-induced charge separation and reactive oxygen species generation. Importantly, incorporating AgNPs into PVA did not sacrifice flexibility but instead enhanced mechanical strength (UTS ~323 MPa), thermal stability, and optical tunability. 2 mg/mL composite film quantitatively achieved a rate constant of 0.024 min^{-1} for MB degradation, a 2 cm inhibition zone against *E.coli* strain, and retained > 85% antibacterial activity after 4 reuse cycles. Future work will include ecotoxicity assessment of Ag^+ leaching in aquatic environments to ensure safe deployment. This green synthesis platform establishes a practical template for sustainable material design, and the next step is integrating this foldable film into a portable flow-through device for real-time field deployment enabling soldiers in remote forests or disaster-relief workers to purify pond water safely and directly, while also serving as an antimicrobial wound dressing. Thus, this work directly bridges laboratory material innovation with pressing environmental and biomedical needs.

CRediT authorship contribution statement

Rajitha Kathi: Formal analysis, Data curation. **GL Merlinsheeba:** Investigation, Data curation. **Ravi Kali:** Investigation. **Balaji Padya:** Writing – review & editing, Investigation. **Nitin P. Wasekar:** Data curation. **Krishnakumar Balu:** Writing – review & editing, Data curation. **Vijay Morampudi:** Writing – review & editing. **Pavan Kumar Jain:** Writing – review & editing. **Parvathalu Kalakonda:** Writing –

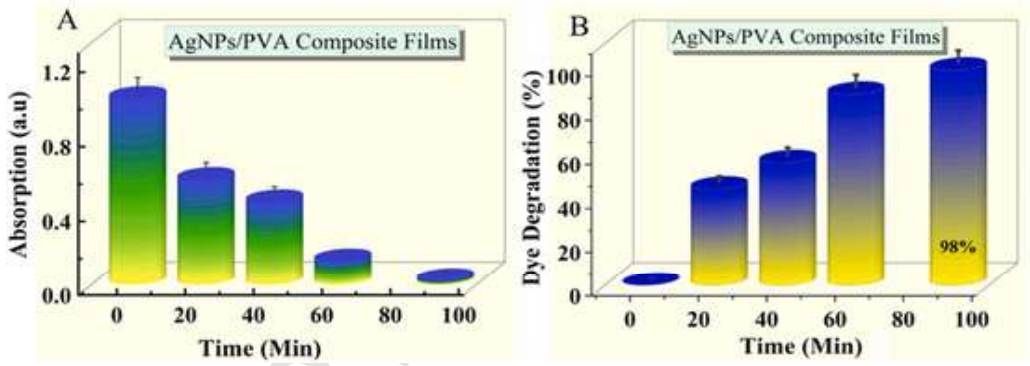

Fig. 12a. Photocatalytic degradation kinetics of methylene blue dye using *Argyreia nervosa*-mediated AgNPs/PVA nanocomposite films (2.4 mg/mL): (A) Time-dependent UV-Vis absorption spectra showing progressive decrease of the characteristic 664 nm peak; (B) Quantitative degradation efficiency achieving 98% MB removal within 90 min under visible light irradiation, demonstrating excellent photocatalytic performance and reusability of the nanocomposite films.

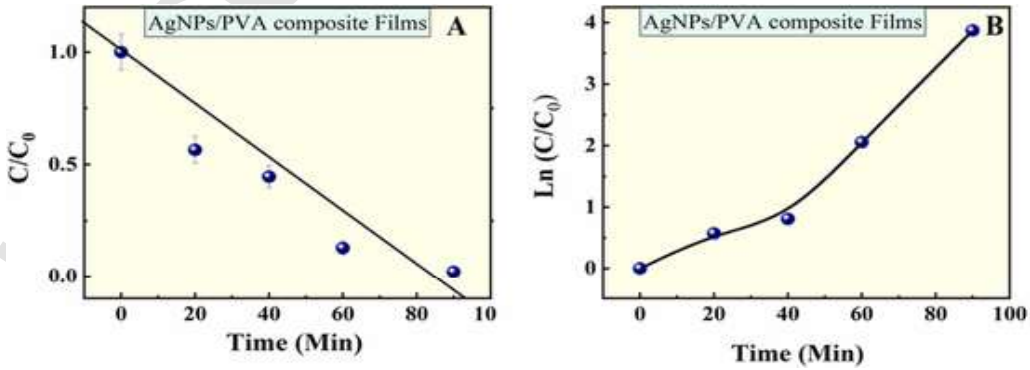

Fig. 12b. Pseudo-first-order kinetic analysis [55] of methylene blue degradation by *Argyreia nervosa*-mediated AgNPs/PVA nanocomposite films, showing linear correlation between $\ln(C_0/C)$ and irradiation time with rate constant k = 0.017 min^{-1} (R^2 = 0.954), confirming the photocatalytic degradation follows Langmuir-Hinshelwood kinetics.

review & editing, Writing – original draft, Supervision, Project administration, Conceptualization.

Ethical approval

The internal review board committee of our lab stated that no ethical approval was required for this study as it did not involve human or animal subjects.

Funding

No funding was received for this project.

Uncited references

[12], [57].

Declaration of Competing Interest

The authors declare that they have no known competing financial interests or personal relationships that could have appeared to influence the work reported in this paper.

Acknowledgements

This research was carried out with the support of the Smart Nanomaterial Research Laboratory (SNRL), Department of Physics, Government City PG College (A), Osmania University, Hyderabad, India.

Data Availability

Data will be made available on request. The data supporting the findings of this study are available from the corresponding author upon reasonable request.

Appendix A. Supporting information

Supplementary data associated with this article can be found in the online version at doi:10.1016/j.mtcomm.2026.115467.

References

[1] V.V. Makarov, et al., Green' nanotechnologies: synthesis of metal nanoparticles using plants, Acta Nat. 6 (2014) 35–44.
[2] K.J. Wolf, J. Chen, J.D. Coombes, M.K. Aghi, S. Kumar, Dissecting and rebuilding the glioblastoma microenvironment with engineered materials, Nat. Rev. Mater. 4 (2019) 651–668.
[3] L. Zhang, J. Zhang, H. Yu, J. Yu, Emerging S-Scheme Photocatalyst, Adv. Mater. 34 (2022) 2107668.
[4] P. Kalakonda, et al., Eco-Friendly Fabrication of Silver Nanoparticles for Sustainable Water Purification and Antibacterial Synergy, Plasmonics 19 (2024) 2857–2869.
[5] Green synthesis of metal nanoparticles and their environmental applications." Journal of Cleaner Production.
[6] M. Kohoutová, Prevention of cell agglutination and competence in a genetically transformable strain of Pneumococcus by D-glucosamine and D-galactosamine, Folia Microbiol. (Praha) 20 (1975) 443–451.
[7] P. Makvandi, et al., Metal-based nanomaterials in biomedical applications: antimicrobial activity and cytotoxicity aspects, Adv. Funct. Mater. 30 (2020) 1910021.
[8] Y. Tominaga, Y. Tsujisaka, Purification and some enzymatic properties of the chitosanase from Bacillus R-4 which lyses Rhizopus cell walls, Biochim. Biophys. Acta 410 (1975) 145–155.
[9] K. Parvathalu, et al., Green Synthesis of Silver Nanoparticles Using Argyreia nervosa Leaf Extract and Their Antimicrobial Activity, Plasmonics 18 (2023) 1075–1081.
[10] Z. Xu, C. Zhang, X. Wang, D. Liu, Release strategies of silver ions from materials for bacterial killing, ACS Appl. Bio Mater. 4 (2021) 3985–3999.
[11] A.S. Sharma, V.S. Sharma, H. Kaur, R.S. Varma, Supported heterogeneous nanocatalysts in sustainable, selective and eco-friendly epoxidation of olefins, Green. Chem. 22 (2020) 5902–5936.
[12] J. Ochs, C.A. Pagnacco, F. Barroso-Bujans, Macrocyclic polymers: synthesis, purification, properties and applications, Prog. Polym. Sci. 134 (2022) 101606.
[13] P. Rujitanaroj, N. Pimpha, P. Supaphol, Wound-dressing materials with antibacterial activity from electrospun gelatin fiber mats containing silver nanoparticles, Polymer 49 (2008) 4723–4732.
[14] P. Kalakonda, S. Banne, Thermomechanical properties of PMMA and modified SWCNT composites, Nanotechnol. Sci. Appl. 10 (2017) 45–52.
[15] P. Kalakonda, S. Banne, P.B. Kalakonda, Study of mechanical anisotropy of single walled carbon nanotube and polyvinyl alcohol polymer nanocomposite with a controlled alignment process, J. Polym. Res. 29 (2022) 442.
[16] Y. Li, W. Zhang, J. Niu, Y. Chen, Mechanism of photogenerated reactive oxygen species and correlation with the antibacterial properties of engineered metal-oxide nanoparticles, ACS Nano 6 (2012) 5164–5173.
[17] Y. Wang, J. He, C. Liu, W.H. Chong, H. Chen, Thermodynamics versus Kinetics in Nanosynthesis, Angew. Chem. Int. Ed. 54 (2015) 2022–2051.
[18] K. Chen, et al., Twofold rigidity activates ultralong organic high-temperature phosphorescence, Nat. Commun. 15 (2024) 1269.
[19] K. Parvathalu, et al., Biomimetic Synthesis of Copper Nanoparticles Using Tinospora Cordifolia Plant Leaf Extract for Photocatalytic Activity Applications, Plasmonics 19 (2024) 825–834.
[20] J. Li, et al., Engineering noble metal nanomaterials for environmental applications, Nanoscale 7 (2015) 7502–7519.
[21] L.J. Jongkind, X. Caumes, A.P.T. Hartendorp, J.N.H. Reek, Ligand Template Strategies for Catalyst Encapsulation, Acc. Chem. Res. 51 (2018) 2115–2128.
[22] A. Sati, T.N. Ranade, S.N. Mali, H.K. Ahmad Yasin, A. Pratap, Silver Nanoparticles (AgNPs): Comprehensive Insights into Bio/Synthesis, Key Influencing Factors, Multifaceted Applications, and Toxicity—A 2024 Update, ACS Omega 10 (2025) 7549–7582.
[23] M.A. Ahmed, S.A. Mahmoud, A.A. Mohamed, Interfacially engineered metal oxide nanocomposites for enhanced photocatalytic degradation of pollutants and energy applications, RSC Adv. 15 (2025) 15561–15603.
[24] S. Chandran, V. Ravichandran, S. Chandran, J. Chemmanda, B. Chandarshekar, Biosynthesis of PVA encapsulated silver nanoparticles, J. Appl. Res. Technol. 14 (2016) 319–324.
[25] M. Harun-Ur-Rashid, T. Foyez, S.B.N. Krishna, S. Poda, A.B. Imran, Recent advances of silver nanoparticle-based polymer nanocomposites for biomedical applications, RSC Adv. 15 (2025) 8480–8505.
[26] A. Bassi, P. Kalakonda, I. Hasan, Synthesis of Chitosan-Agar immobilized NiO-MgO bionanocomposites and their photocatalytic application towards toxic azo dye, Inorg. Chem. Commun. 170 (2024) 113499.
[27] N.K. Dabbeta, et al., Eco-inspired Cu-Zn bimetallic nanoparticles for Enhanced Water Purification Technologies, Mater. Chem. Phys. Sustain. Energy 2 (2025) 100013.
[28] P. Kalakonda, et al., Argyreia nervosa-driven biosynthesis of Cu–Ag bimetallic nanoparticles from plant leaves extract unveils enhanced antibacterial properties, Bioprocess. Biosyst. Eng. 47 (2024) 1307–1319.
[29] M. Valodkar, S. Modi, A. Pal, S. Thakore, Synthesis and anti-bacterial activity of Cu, Ag and Cu–Ag alloy nanoparticles: A green approach, Mater. Res. Bull. 46 (2011) 384–389.
[30] A.G. El-Shamy, W. Attia, K.M. Abd El-Kader, The optical and mechanical properties of PVA-Ag nanocomposite films, J. Alloy. Compd. 590 (2014) 309–312.
[31] A. Khlyustova, N. Sirotkin, A. Kraev, A. Agafonov, V. Titov, Composites based on PVA and Al–Zn structures with excellent mechanical properties, Polym. Compos. 43 (2022) 4029–4037.
[32] L. Hao, et al., Large ultrathin polyoxomolybdate-decorated boron nitride nanosheets with enhanced antibacterial activity for infection control, ACS Appl. Nano Mater. 6 (2023) 4754–4769.
[33] L. Liu, et al., Dynamic nanoconfinement enabled highly stretchable and supratough polymeric materials with desirable healability and biocompatibility, Adv. Mater. 33 (2021) 2105829.
[34] P. Kalakonda, et al., Comparison of Multi-metallic Nanoparticles-Alternative Antibacterial Agent: Understanding the Role of Their Antibacterial Properties, J. Inorg. Organomet. Polym. Mater. 34 (2024) 2203–2218.
[35] S. Shahzadi, S. Fatima, Z. Shafiq, M.R.S.A. Janjua, A review on green synthesis of silver nanoparticles (SNPs) using plant extracts: a multifaceted approach in photocatalysis, environmental remediation, and biomedicine, RSC Adv. 15 (2025) 3858–3903.
[36] S. Smonia Joe Princy, et al., Synergistic Antimicrobial and Photocatalytic Properties of PVP-Ag-PEG Nanocomposites for Sustainable Leachate Treatment, J. Inorg. Organomet. Polym. Mater. (2024) 1–19.
[37] S. Abdollahi, H. Raissi, F. Farzad, Examine stability polyvinyl alcohol-stabilized nanosuspensions to overcome the challenge of poor drug solubility utilizing molecular dynamic simulation, Sci. Rep. 14 (2024) 17386.
[38] K.K. Sadasivuni, et al., Silver nanoparticles and its polymer nanocomposites—synthesis, optimization, biomedical usage, and its various applications, in: Polymer nanocomposites in biomedical engineering, Springer, 2019, pp. 331–373.
[39] T.D. Hoang, et al., Preparation and photocatalytic and antibacterial properties of polyvinyl alcohol/chitosan/TiO2@Ag electrospun nanofibers, Thin Solid. Films 797 (2024) 140344.
[40] S. B. Aziz, et al., Fabrication of interconnected plasmonic spherical silver nanoparticles with enhanced localized surface plasmon resonance (LSPR) peaks using quince leaf extract solution, Nanomaterials 9 (2019) 1557.
[41] R. Alipour, A. Khorshidi, A.F. Shojaei, F. Mashayekhi, M.J.M. Moghaddam, Skin wound healing acceleration by Ag nanoparticles embedded in PVA/PVP/Pectin/Mafenide acetate composite nanofibers, Polym. Test. 79 (2019) 106022.
[42] H.S. Mansur, C.M. Sadahira, A.N. Souza, A.A.P. Mansur, FTIR spectroscopy characterization of poly (vinyl alcohol) hydrogel with different hydrolysis degree

and chemically crosslinked with glutaraldehyde, Mater. Sci. Eng. C. 28 (2008) 539–548.
[43] S.D. Desai, et al., Cross-linking of poly (vinyl alcohol) films under acidic and thermal stress, Eur. J. Pharm. Sci. 152 (2020) 105429.
[44] N.Q. Vu, et al., Engineering Functional PVA: A Comprehensive Review of Chemical Modifications and Prospective Developments, ACS Polym. Au 6 (2026) 33–60.
[45] A. Ekinci, A.A. Johnson, A. Gleadall, X. Han, The effect of geometry on tensile strength of biodegradable polylactic-acid tensile-test specimens by material extrusion, Int. J. Rapid Manuf. 10 (2021) 23–35.
[46] J.A. Hindler, A.H. González, T.A. Drake, Stability of viable-bacterium counts in liquid media used for preparation of inocula and subsequent impact on antimicrobial susceptibility test results, J. Clin. Microbiol. 28 (1990) 1271–1275.
[47] P. Petchsong, T. Rattanawongwiboon, S. Ummartyotin, Gamma-Irradiated PVA/Bacterial Cellulose Aerogels as Ethylene Scavengers for Climacteric Fruit Preservation, Carbohydr. Polym. Technol. Appl. (2026) 101144, https://doi.org/10.1016/j.carpta.2026.101144.
[48] J.J. Mock, M. Barbic, D.R. Smith, D.A. Schultz, S. Schultz, Shape effects in plasmon resonance of individual colloidal silver nanoparticles, J. Chem. Phys. 116 (2002) 6755–6759.
[49] K.A. Willets, R.P. Van Duyne, Localized Surface Plasmon Resonance Spectroscopy and Sensing, Annu. Rev. Phys. Chem. 58 (2007) 267–297.
[50] C. Zhang, Q. Tu, L.F. Francis, U.R. Kortshagen, Band gap tuning of films of undoped zno nanocrystals by removal of surface groups, Nanomaterials 12 (2022) 565.
[51] M. Krysa, M. Szymańska-Chargot, A. Zdunek, FT-IR and FT-Raman fingerprints of flavonoids–a review, Food Chem. 393 (2022) 133430.
[52] S. Mustapha, et al., Comparative study of crystallite size using Williamson-Hall and Debye-Scherrer plots for ZnO nanoparticles, Adv. Nat. Sci. Nanosci. Nanotechnol. 10 (2019) 045013.
[53] T.C. Dakal, A. Kumar, R.S. Majumdar, V. Yadav, Mechanistic basis of antimicrobial actions of silver nanoparticles, Front. Microbiol. 7 (2016) 1831.
[54] I. Sondi, B. Salopek-Sondi, Silver nanoparticles as antimicrobial agent: a case study on E. coli as a model for Gram-negative bacteria, J. Colloid Interface Sci. 275 (2004) 177–182.
[55] J.-P. Simonin, On the comparison of pseudo-first order and pseudo-second order rate laws in the modeling of adsorption kinetics, Chem. Eng. J. 300 (2016) 254–263.
[56] M. Behnajady, N. Modirshahla, R. Hamzavi, Kinetic study on photocatalytic degradation of C.I. Acid Yellow 23 by ZnO photocatalyst, J. Hazard. Mater. 133 (2006) 226–232.
[57] X. Ji, et al., TiO2/Ag nanoparticles)@(chitosan-polyvinyl alcohol) core-shell nanofibers as novel anticorrosion and antibacterial improvers for epoxy coating systems, J. Polym. Res. 30 (2023) 244.